

Phase-sensitive atom localization for closed-loop quantum systems

H. R. Hamedī* and Gediminas Juzeliūnas†

Institute of Theoretical Physics and Astronomy, Vilnius University, Saulėtekio 3, Vilnius 10222, Lithuania

(Received 2 December 2015; published 25 July 2016)

A scheme of high-precision two- and three-dimensional (3D) atom localization is proposed and analyzed by using a density matrix method for a five-level atom-light coupling scheme. In this system four strong laser components (which could be standing waves) couple a pair of atomic internal states to another pair of states in all possible ways to form a closed-loop diamond-shape configuration of the atom-light interaction. By systematically solving the density matrix equations of the motion, we show that the imaginary part of the susceptibility for the weak probe field is position dependent. As a result, one can obtain information about the position of the atom by measuring the resulting absorption spectra. Focusing on the signatures of the relative phase of the applied fields stemming from the closed-loop structure of the diamond-shape subsystem, we find out that there exists a significant phase dependence of the eigenvalues required to have a maximum in the probe absorption spectra. It is found that by properly selecting the controlling parameters of the system, a nearly perfect 2D atom localization can be obtained. Finally, we numerically explore the phase control of 3D atom localization for the present scheme and show the possibility to obtain 1/2 detecting probability of finding the atom at a particular volume in 3D space within one period of standing waves.

DOI: [10.1103/PhysRevA.94.013842](https://doi.org/10.1103/PhysRevA.94.013842)

I. INTRODUCTION

It is known from the early days of quantum mechanics that the Heisenberg microscope [1] imposes the limitation that the atomic position cannot be detected more precisely than the half wavelength of radiation used for the detection. In the archetype of this measuring device, based on the uncertainty principle $\Delta p_x \Delta x \sim \hbar$, the largest momentum kick transferred from an optical photon to an atom $\Delta p_x = 2\hbar k$, indicates the precision in the measurement of the atomic position in terms of the optical wavelength $\lambda = 2\pi/k$ as $\Delta x \sim \lambda/2$. Following these arguments the atom cannot be localized within distances beyond the optical half wavelength. However, novel localization techniques have made it possible to overcome this fundamental limit, and extremely high-precision spatial resolutions have been achieved for measurement of the atomic position. For instance, Gorshkov *et al.* [2] suggested a method based on a dark state to localize an atomic excitation with resolution that approaches a few nanometers. The Scully group reported experimentally the first proof of dark-state-based localization in a Rb vapor cell [3]. Recently, Miles and coworkers have demonstrated an experiment in which the atomic excitation is confined to a spatial width of 100 nm, which is a factor of 8 smaller than the wavelength of the laser beams used in their experiment [4]. Precision position measurement of an atom is useful in neutral atom lithography with ultrahigh resolution [5], measurement of the center-of-mass wave function of moving atoms [6], and coherent patterning of matter waves [7].

Earlier theoretical studies for the localization mostly consider one-dimensional (1D) atom localization based on the atomic coherence and quantum interference effects [8–12]. Note that the quantum coherence and interference play a fundamental role in many other phenomena of atomic physics

and quantum optics, such as an electromagnetically induced transparency (EIT) [13–18], superluminal light propagation [19–22], optical bistability [23,24], Kerr nonlinearity [25,26], and others [27–29]. More recently, some schemes have been put forward for two-dimensional (2D) atom localization [30–42]. Ding *et al.* [31] investigated the atom localization by monitoring the probe absorption in a microwave-driven four-level atomic medium affected by two orthogonal standing-wave fields. They found that the localization behavior is significantly improved due to a joint quantum interference induced by a standing-wave and microwave-driven fields. In another work, an *M*-type atomic system was proposed by the same group [32] to deal with the 2D atom localization in the subwavelength domain via a controlled spontaneous emission. Wan *et al.* [38] considered an atomic scheme based on the controlled probe absorption and gain in a four-level double Λ system. They showed both numerically and analytically that the high-precision atom localization achieved in such a scheme can be attributed to the interference between the one- and three-photon excitations. A four-level tripod-type atomic system is also proposed to achieve a high-precision two-dimensional atom localization via measurement of the excited state population [40]. Yet the three-dimensional (3D) atom localization has been investigated only in few proposals [43–45]. Compared to the 1D and 2D localization, the 3D localization of an atom gives a more specific information about the position of a moving atom.

In this paper we investigate the 2D and 3D localization of an atom in a five-level configuration in which the laser beams couple the ground level to a four-level closed-loop system. Such a scheme was first proposed by Kobrak and Rice [46] for establishing a complete population transfer [47,48] to a single target of a degenerate pair of states. Subsequently it has been employed to show the advantages of the measurement in coherent control of atomic or molecular processes [49]. Moreover, by using intense laser fields a new quantum measurement has been introduced in the Kobrak-Rice (KR5) system [50]. Recently, this scheme has been employed by us

*hamid.hamedi@tfai.vu.lt

†gediminas.juzeliunas@tfai.vu.lt

to study the behavior of the third-order susceptibility [26]. It has been shown that under the condition of the multiphoton resonance, one can enhance the Kerr nonlinearity of such a five-level medium by properly adjusting the amplitudes and phases of the applied fields, so that the linear and nonlinear absorption reduce considerably in a region with a positive group velocity.

Here we make use of the KR5 scheme to localize atoms in two and three dimensions. We employ three different situations in which the atom could interact with the position-dependent standing-wave fields. In the first two cases all four laser fields represent the standing waves, whereas in the third case only one of the fields is a standing wave, others being propagating waves. It is shown that one can extract information about the position of the atom through measuring the probe absorption. Since the KR5 atomic scheme is phase sensitive, the phase control of atom localization is also possible by adjusting properly the relative phase. In particular, by properly choosing the amplitudes and phases of the driving fields, the atom-light Hamiltonian can have three, four, and two eigenstates, resulting in different localization patterns in the probe absorption spectrum. Subsequently it is demonstrated that the first two atom-field coupling situations are not suitable to achieve a unique atom localization peak. In order to obtain the maximum detection probability of the atom at a certain position in the 2D space, we consider the next situation of coupling between atom and standing-wave fields, and illustrate that the maximal probability of finding the atom in one period of standing waves reaches the unity. Eventually, the phase control of the 3D atom localization for this five-level scheme is explored numerically in the 3D space. It is found that the detection probability of finding the atom in a particular volume in 3D space and within one period of standing waves can become 50%.

II. MODEL AND EQUATIONS

The proposed KR5 five-level scheme is illustrated in Fig. 1(a). The system consists of an excited state $|1\rangle$, two nondegenerate metastable lower states $|3\rangle$ and $|5\rangle$, as well as two intermediate degenerate states $|4\rangle$ and $|2\rangle$. Four coherent laser driving components Λ_{43} , Λ_{32} , Λ_{41} , and Λ_{21} are applied to couple a pair of atomic internal states $|1\rangle$ and $|3\rangle$ to another pair of states $|4\rangle$ and $|2\rangle$ in all possible ways to form a closed-loop scheme of the atom-light interaction. The transition between the states $|3\rangle$ and $|5\rangle$ is dipole allowed. Such a configuration is equivalent to a cyclical coupling of four states $|1\rangle$, $|2\rangle$, $|3\rangle$, and $|4\rangle$, making a diamond-shaped closed-loop system. By applying a weak coherent probe field with a Rabi frequency Ω_p , the diamond-shaped system is coupled to a ground or metastable state $|5\rangle$.

The atom moves along the z direction and interacts with driving laser fields propagating in the x - y plane. The laser radiation can be traveling or standing waves. In the latter case the strength of the interaction between the atom and the standing-wave fields is spatially dependent. The atom is assumed to move with a high enough velocity so that its interaction with the driving fields does not affect its motion in the z direction. Thus, we may treat the atomic motion classically characterized by a constant velocity in the z

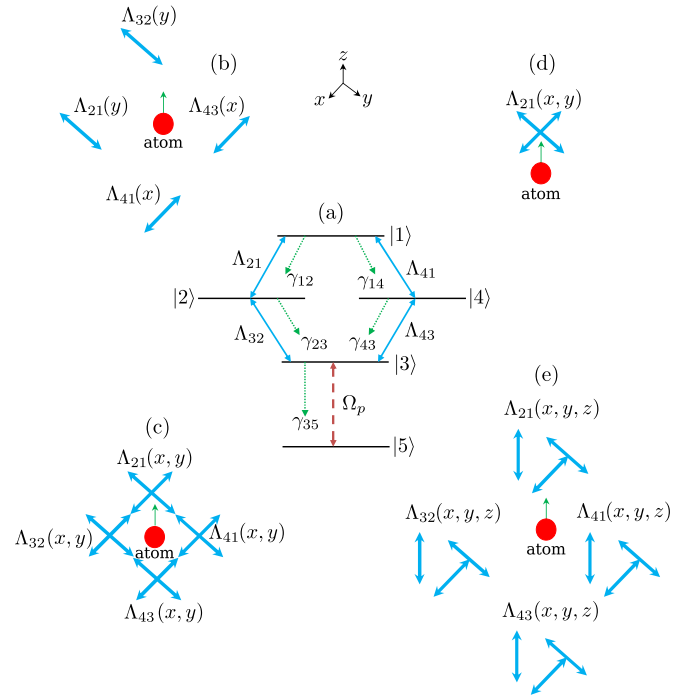


FIG. 1. (a) Schematic diagram of the five-level quantum system. (b), (c), (d), and (e) Different situations considered in which the atom could interact with the position-dependent standing-wave fields.

direction. On the other hand, the center-of-mass position of the atom along the directions of standing waves (in the x - y plane) can experience only the minor changes and thus remains nearly constant. In this case, one can neglect the kinetic energy term of the atom in the interaction Hamiltonian via the Raman-Nath approximation [51]. Then, applying the rotating-wave approximation, the resulting interaction Hamiltonian for the whole system can be written as

$$\begin{aligned}
H_{5\text{Levels}} = & -\hbar(\Omega_p|3\rangle\langle 5| + \Lambda_{41}|1\rangle e^{i\phi}\langle 4| \\
& + \Lambda_{21}|2\rangle\langle 1| + \Lambda_{32}|3\rangle\langle 2| + \Lambda_{43}|4\rangle\langle 3|) \\
& + \text{H.c.}, \tag{1}
\end{aligned}$$

where $\phi = \phi_{41} + \phi_{43} - \phi_2 - \phi_{21}$ is a relative phase accumulated after completing a cyclic loop and ϕ_{ij} represents the initial phase of the laser field, which induces the transition $|i\rangle \longleftrightarrow |j\rangle$. The equation of the motion for the density operator of the atomic system is given by:

$$\dot{\rho} = -\frac{i}{\hbar}[H_{5\text{Levels}}, \rho] + L_\rho, \tag{2}$$

where the a damping operator L_ρ represented the decay of the system. Substituting (1) into (2), one arrives at the optical Bloch equations for density matrix elements of the five-level system [26].

Our aim is to acquire information about the position of the atom passing through the standing-wave fields from the absorption of the probe field

$$\chi'' = \text{Im}(\chi), \tag{3}$$

where [52]

$$\chi = \frac{2N\mu_{53}^2}{\varepsilon_0\hbar\Omega_p}\rho_{35}. \quad (4)$$

is a linear susceptibility of the system for the probe field, and N is the atomic number density. Therefore the absorption measurements allow us to determine the off-diagonal density-matrix element ρ_{35} featured in Eq. (4).

For a weak intensity of the probe field, the atom populates predominantly the initially populated ground state $|5\rangle$, so that $\rho_{55} \approx 1$. Under this condition, the density matrix equations can be simplified by writing them in the matrix form

$$\dot{R} = -MR + A, \quad (5)$$

where R , A , and M are given by

$$R = \begin{pmatrix} \rho_{35} \\ \rho_{45} \\ \rho_{25} \\ \rho_{15} \end{pmatrix}, \quad (6)$$

$$A = \begin{pmatrix} i\Omega_p \\ 0 \\ 0 \\ 0 \end{pmatrix}, \quad (7)$$

and

$$M = \begin{pmatrix} S_1 & -i\Lambda_{43} & -i\Lambda_{32} & 0 \\ -i\Lambda_{43} & S_2 & 0 & -i\Lambda_{41}e^{-i\phi} \\ -i\Lambda_{32} & 0 & S_3 & -i\Lambda_{21} \\ 0 & -i\Lambda_{41}e^{i\phi} & -i\Lambda_{21} & S_4 \end{pmatrix}, \quad (8)$$

with $S_1 = \gamma_{35} - i\Delta_p$, $S_2 = i(\Delta_{43} + \Delta_p) - \gamma_{43}$, $S_3 = -[i(\Delta_{23} - \Delta + \Delta_p) - \gamma_{23}]$, and $S_4 = -[i(\Delta_{14} + \Delta_{43} + \Delta_p) - (\gamma_{14} + \gamma_{12})]$. Here the parameter $\Delta = \Delta_{12} - \Delta_{14} + \Delta_{23} - \Delta_{43}$ describes a multiphoton detuning. On the other hand, $\Delta_p = \omega_p - \omega_{35}$, $\Delta_{43} = \omega_4 - \omega_{43}$, $\Delta_{23} = \omega_2 - \omega_{23}$, $\Delta_{14} = \omega_3 - \omega_{14}$, and $\Delta_{12} = \omega_1 - \omega_{12}$ are, respectively, the frequencies of the one photon detuning for the transitions $|3\rangle \longleftrightarrow |5\rangle$, $|4\rangle \longleftrightarrow |3\rangle$, $|2\rangle \longleftrightarrow |3\rangle$, $|1\rangle \longleftrightarrow |4\rangle$, and $|2\rangle \longleftrightarrow |1\rangle$, with ω_i being the central frequency of the laser fields. The rates of the spontaneous decay from upper level $|i\rangle$ to the lower level $|j\rangle$ is given by $2\gamma_{ij}$. Furthermore, we did not include the spontaneous decay from the excited state $|1\rangle$ to the lower levels $|3\rangle$ and $|5\rangle$ assuming that the corresponding transitions are dipole forbidden.

The steady-state solution to Eq. (5) reads in the matrix form

$$R = M^{-1}A. \quad (9)$$

Using Eq. (9), the coherence term ρ_{35} can be expressed as

$$\rho_{35} = i\Omega_p \frac{S_2\Lambda_{21}^2 + S_3\Lambda_{41}^2 + S_2S_3S_4}{Z}, \quad (10)$$

where

$$\begin{aligned} Z = & 2\Lambda_{41}\Lambda_{32}\Lambda_{43}\Lambda_{21}\cos\phi \\ & + S_2S_4\Lambda_{32}^2 - S_3S_4\Lambda_{43}^2 \\ & - S_1S_2\Lambda_{21}^2 + S_1S_3\Lambda_{41}^2 \\ & - \Lambda_{43}^2\Lambda_{21}^2 - \Lambda_{41}^2\Lambda_{32}^2 - S_1S_2S_3S_4, \end{aligned} \quad (11)$$

It is apparent that the phase factor enters the absorption through the term $2\Lambda_{41}\Lambda_{32}\Lambda_{43}\Lambda_{21}\cos\phi$.

Equation (10) represents a main result of the paper allowing one to measure the position of the atom via the absorption of the atomic system given by the imaginary part of ρ_{35} featured in Eqs. (3) and (4). Equation (10) shows that the absorption depends on the parameters of the system, i.e., the amplitudes of the standing-wave fields, relative phase of applied fields, as well as the detunings of the probe and driving fields. We will discuss this issue in more detail in the following section.

III. NUMERICAL RESULTS AND DISCUSSION

Now, we investigate the localization of the atom through numerical results by considering different cases of interaction of the atom with the laser fields. The simulations are displayed in the units of $\frac{2N\mu_{53}^2}{\varepsilon_0\hbar\Omega_p}$. The selected parameters are $\gamma_{14} = \gamma_{12} = \gamma_{23} = \gamma_{43} = \gamma_{35} = \gamma$, and all the parameters are scaled with γ . Note that the wave number of optical waves are selected to be the same and equal to k .

A. 2D atom localization

1. First case: All control fields are position dependent in one dimension

Considering the case where the different atomic transitions are coupled by different orthogonal standing-wave fields [Fig. 1(b)], the resulting Rabi frequencies are

$$\begin{aligned} \Lambda_{43} &= \Lambda_{43}(x, y) = \Omega_{43}f_{11}(x), \\ \Lambda_{41} &= \Lambda_{41}(x, y) = \Omega_{41}f_{11}(x), \\ \Lambda_{32} &= \Lambda_{32}(x, y) = \Omega_{32}f_{12}(y), \\ \Lambda_{21} &= \Lambda_{21}(x, y) = \Omega_{21}f_{12}(y), \end{aligned} \quad (12)$$

with

$$\begin{aligned} f_{11}(x, y) &= \sin(kx), \\ f_{12}(x, y) &= \sin(ky), \end{aligned} \quad (13)$$

It can be seen from Eqs. (3), (4), (10), and (12) that the probe absorption χ'' is position dependent. As a result, by measuring probe absorption spectra χ'' one can obtain information about the position of the atom in the x - y plane as it passes through the standing wave fields. The position of the peak in the probe absorption specifies the location of the atom during its optical detection. Four different patterns of 2D atom localization are illustrated in Fig. 2. As it can be seen from Fig. 2(a), when $\Omega_{43} = \Omega_{32} = \Omega_{41} = \Omega_{21} = 5\gamma$ and $\phi = 0$, the probe absorption maxima displays four craterlike patterns at each quadrant, and the atom is localized at these circles. For $\Omega_{32} = \Omega_{21} = \Omega_1 \neq \Omega_2 = \Omega_{43} = \Omega_{41}$ the craterlike patterns gradually move closer to each other and change to the patterns with a shape resembling the number 8. When $\Omega_2 > \Omega_1$ [Fig. 2(b)], the patterns are along the x direction, while as shown in Fig. 2(c) for $\Omega_2 < \Omega_1$, they are along the y direction. As illustrated in Fig. 2(d), for $\phi = \pi$, the 2D atom localization pattern changes totally with respect to Fig. 2(a). In all the cases, the maximum probability of atom at a particular position is $1/4$.

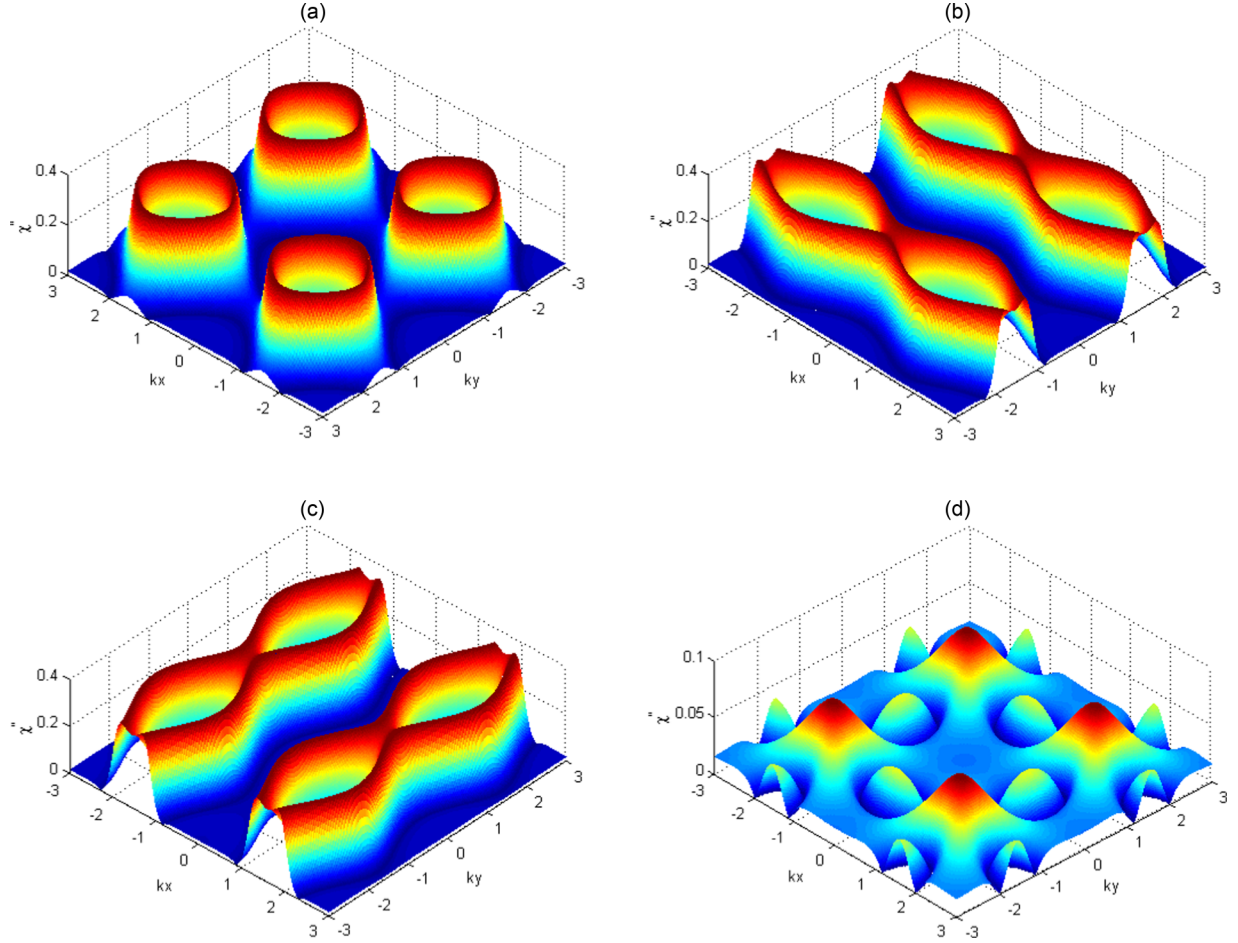


FIG. 2. Plots of probe absorption χ'' versus (k_x, k_y) . The selected parameters are $(\Omega_{43}, \Omega_{32}, \Omega_{41}, \Omega_{21}, \phi) =$ (a) $(5\gamma, 5\gamma, 5\gamma, 5\gamma, 0)$, (b) $(4\gamma, 6\gamma, 4\gamma, 6\gamma, 0)$, (c) $(6\gamma, 4\gamma, 6\gamma, 4\gamma, 0)$, (d) $(5\gamma, 5\gamma, 5\gamma, 5\gamma, \pi)$. The other parameters are $\gamma_{14} = \gamma_{12} = \gamma_{23} = \gamma_{43} = \gamma_{35} = \gamma$, $\Delta = \Delta_{12} = \Delta_{14} = \Delta_{23} = \Delta_{43} = 0$, as well as $\Delta_p = 8\gamma$, $\Omega_p = 0.01\gamma$.

2. Second case: All control fields are position dependent in two dimensions

Let us consider now a situation where each standing-wave field is obtained from a superposition of two orthogonal standing-wave fields with the same frequency along the directions x and y [Fig. 1(c)]. As a result, the Rabi frequencies of standing waves are position dependent and are given by

$$\begin{aligned}\Lambda_{43} &= \Lambda_{43}(x, y) = \Omega_{43} f_2(x, y), \\ \Lambda_{41} &= \Lambda_{41}(x, y) = \Omega_{41} f_2(x, y), \\ \Lambda_{32} &= \Lambda_{32}(x, y) = \Omega_{32} f_2(x, y), \\ \Lambda_{21} &= \Lambda_{21}(x, y) = \Omega_{21} f_2(x, y),\end{aligned}\quad (14)$$

with

$$f_2(x, y) = \sin(kx) + \sin(ky). \quad (15)$$

In Fig. 3, we show our simulations for the 2D atom localization by proper adjusting the four standing-wave fields. As shown in Fig. 3(a), for the case where $\Omega_{43} = \Omega_{32} = \Omega_{41} = \Omega_{21} = 10\gamma$, the probe-absorption maxima are distributed in all quadrants of the x - y plane and with a latticelike structure. Setting $(\Omega_{43}, \Omega_{32}, \Omega_{41}, \Omega_{21}) = (8\gamma, \gamma, 10\gamma, 10\gamma)$, the 2D spatial distribution of the atom is almost the same as the one in

Fig. 3(a), but with two spikelike peaks located in quadrants I and III [Fig. 3(b)]. We observe that for the condition $\Omega_{43} = \Omega_{32} = \Omega_{41} = \Omega_{21} = 25\gamma$ corresponding to Fig. 3(c), the resulting absorption spectrum is similar to that in Fig. 3(a). For all these cases [Figs. 3(a)–3(c)], the information on the position of the atom in the x - y plane is ambiguous. A better spatial resolution in the distribution of the probe absorption of the atom can be obtained by adjusting the standing wave intensities to $\Omega_{43} = \Omega_{32} = \Omega_{41} = \Omega_{21} = 2.5\gamma$. In this case, as it can be observed from Fig. 3(d), the probe absorption shows two spikelike atom localization peaks in the first and third quadrants. Therefore, the uncertainty in position measurement of the atom is reduced compared to the previous cases shown in Figs. 3(a)–3(c), and the detection probability of the atom in one period of the standing-wave fields becomes approximately $1/2$.

Next, we intend to investigate the influence of relative phase ϕ on precision in the position measurement of the atom in the x - y plane. Equations (10) and (11) show that the probe absorption is sensitive to the relative phase of the applied fields ϕ through the term $\cos \phi$. Here, we present an analytical model to elucidate such a phase-sensitive property. Four driving fields acting on the atom provide a closed-loop (ring coupling) level scheme in which the relative phase between driving fields affects the probe absorption χ'' . Excluding the ground (or

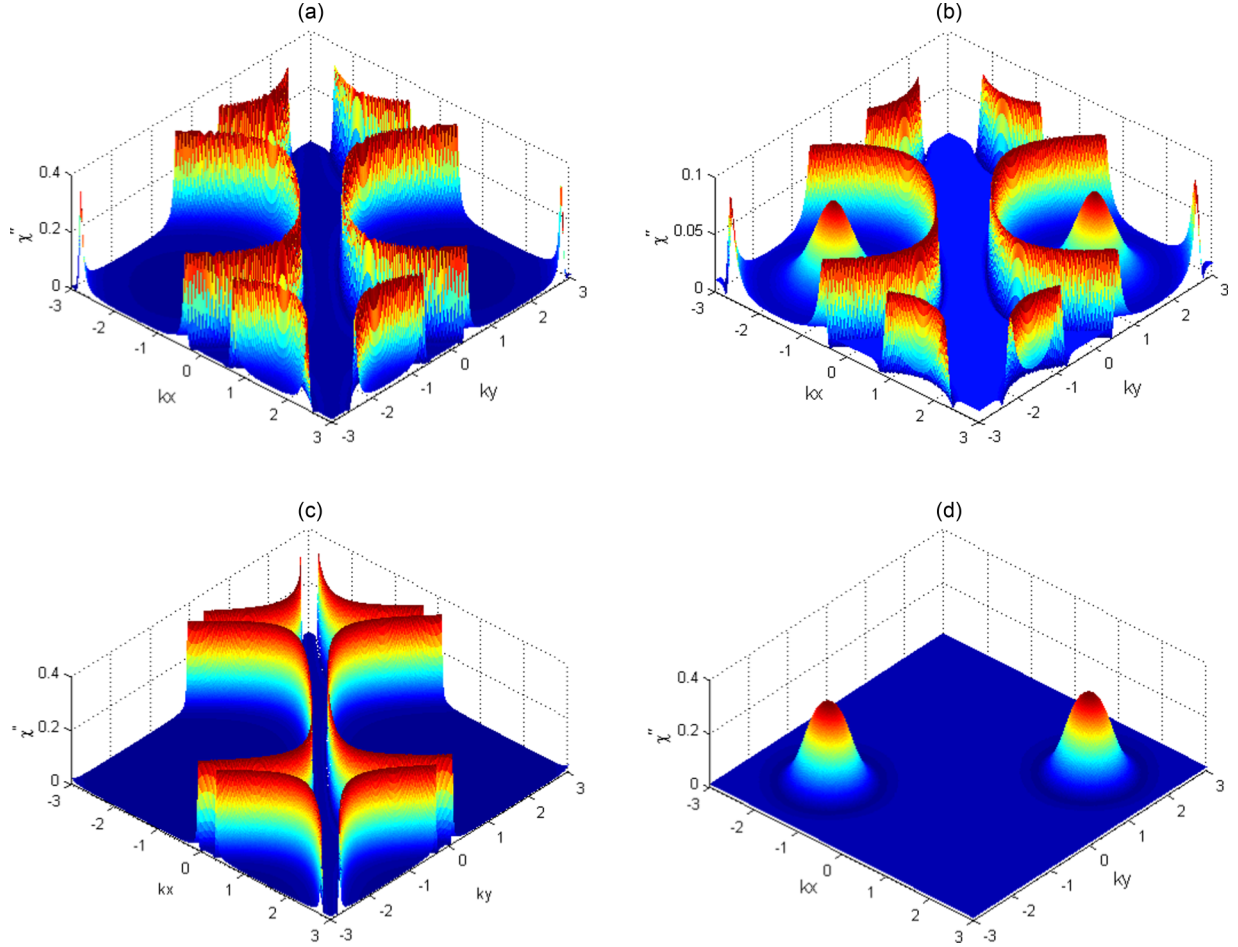


FIG. 3. Plots of probe absorption χ'' versus (kx, ky) . The selected parameters are $(\Omega_{43}, \Omega_{32}, \Omega_{41}, \Omega_{21}) =$ (a) $(10\gamma, 10\gamma, 10\gamma, 10\gamma)$, (b) $(8\gamma, \gamma, 10\gamma, 10\gamma)$, (c) $(25\gamma, 25\gamma, 25\gamma, 25\gamma)$, (d) $(2.5\gamma, 2.5\gamma, 2.5\gamma, 2.5\gamma)$. Here, $\Delta_p = 10\gamma$, $\phi = 0$. The other parameters are the same as Fig. 2.

metastable) state $|5\rangle$ in Eq. (1), one can rewrite the Hamiltonian of the atom-light interaction for the remain atomic four-level closed-loop level structure of the diamond shape as:

$$H_{4\text{Levels}} = -\hbar\Lambda(x, y) \left[|1\rangle e^{i\phi} \langle 4| + \sum_{j=1}^3 |j+1\rangle \langle j| + \text{H.c.} \right], \quad (16)$$

where we have taken $\hbar = 1$. Note that in this equation all the position-dependent Rabi frequencies are chosen to be the same; i.e. $\Lambda_{43}(x, y) = \Lambda_{23}(x, y) = \Lambda_{41}(x, y) = \Lambda_{21}(x, y) = \Lambda(x, y) = \Omega[\sin(kx) + \sin(ky)]$.

The Hamiltonian Eq. (16) is equivalent to an infinite translationally symmetric Hamiltonian

$$H_{4\text{Levels}} = -\Lambda(x, y) \sum_{j=-\infty}^{\infty} |j+1\rangle \langle j| + \text{H.c.}, \quad (17)$$

as long as the coefficients c_j entering any state vector $|\dots\rangle = \sum_j c_j |j\rangle$ obey the boundary conditions

$$c_{j+4} = e^{i\phi} c_j. \quad (18)$$

When $\phi = 0$, Eq. (18) reduces to the usual periodic boundary conditions. On the other hand, for $\phi = \pm\pi$ Eq. (18) represents the twisted boundary conditions.

The Hamiltonian given by Eq. (16) can be easily diagonalized [53], and its eigenstates and corresponding eigenenergies read:

$$|n(r)\rangle = \frac{1}{2} \sum_{j=1}^4 |j\rangle e^{iq_n j}, \quad (19)$$

and

$$E_n = -2\Omega \cos q_n [\sin(kx) + \sin(ky)], \quad (20)$$

where $n = 1, 2, 3, 4$. The dimensionless parameter q_n takes a set of values, which depend on the relative phase ϕ due to the boundary condition Eq. (18):

$$q_n = \frac{(n-1)\pi}{2} - \frac{\phi}{4}, \quad (21)$$

with $(n = 1, 2, 3, 4)$. It can be seen through Eqs. (20) and (21) that the position-dependent eigenenergies depend strongly on the relative phase ϕ .

Let now analyze the eigenenergies for different phase ϕ . For condition $\phi = 0$, Eq. (20) changes to

$$E_n = -2\Omega \sin\left(\frac{n\pi}{2}\right) [\sin(kx) + \sin(ky)]. \quad (22)$$

Equation (22) results in three eigenenergies $E_3 = -E_1 = 2\Omega[\sin(kx) + \sin(ky)]$, and $E_2 = E_4 = 0$. When $\phi = \pi/2$, we

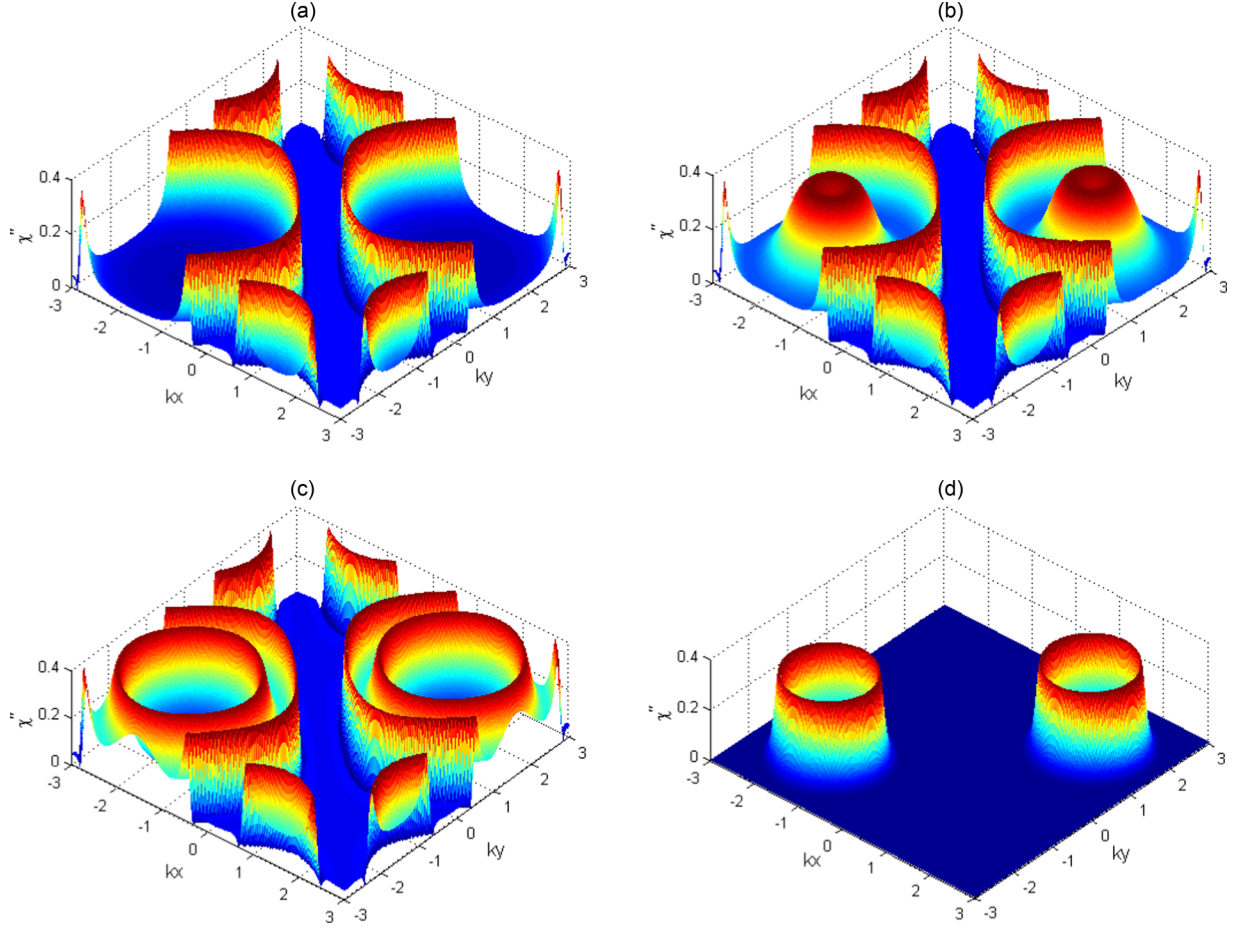


FIG. 4. Plots of probe absorption χ'' versus (kx, ky) . The selected parameters are (a) $\phi = 0$, (b) $\phi = \pi/3$, (c) $\phi = \pi/2$, (d) $\phi = \pi$. Here, $(\Omega_{43}, \Omega_{32}, \Omega_{41}, \Omega_{21}) = (5\gamma, 5\gamma, 5\gamma, 5\gamma)$, $\Delta_p = 5\gamma$. The other parameters are the same as Fig. 4.

obtain

$$E_n = -2\Omega \sin\left(\frac{n\pi}{2} - \frac{\pi}{8}\right) [\sin(kx) + \sin(ky)]. \quad (23)$$

Equation (23) gives the following four eigenenergies: $E_3 = -E_1 = 4\Omega[\sin(kx) + \sin(ky)] \cos \frac{\pi}{8}$, and $E_4 = -E_2 = 4\Omega[\sin(kx) + \sin(ky)] \sin \frac{\pi}{8}$. Finally, for $\phi = \pi$, Eq. (20) reduces to

$$E_n = -2\Omega \sin\left(\frac{n\pi}{2} - \frac{\pi}{4}\right) [\sin(kx) + \sin(ky)]. \quad (24)$$

In such a case one arrives at two pairs of degenerate eigenenergies $E_1 = E_2 = -\sqrt{2}\Omega[\sin(kx) + \sin(ky)]$, and $E_3 = E_4 = \sqrt{2}\Omega[\sin(kx) + \sin(ky)]$.

Equations (22)–(24) imply that there is a strong phase dependence of the eigenvalues required to achieve maximum in the probe absorption. It can be seen that the number of absorption peaks varies by changing ϕ . Obviously, three, four, and two absorption peaks appear for $\phi = 0$, $\phi = \pi/2$, and $\phi = \pi$, respectively.

Another interesting illustration of our results can be described using the right-hand side of Eqs. (22)–(24). For a given probe detuning, the maximum conditions would be satisfied just when the curves of the probe detuning intersect with the curves obtained from the solutions of Eqs. (22)–(24). There are certain positions in the x - y plane at which probe absorption

maxima take place. The position of intersections depend strongly on the value of the arbitrary selected detunings, as well as on the relative phase ϕ of the applied fields. In this case, the positions of intersections correspond to the probe absorption maxima in the 2D localization patterns illustrated in Fig. 4.

The above discussion implies the dependence of probe absorption χ'' on the relative phase ϕ resulting in different patterns in the 2D localization profile of an atom as demonstrated in Fig. 4. It is found from Figs. 4(a) and 4(b) that for $\phi = 0$ and $\phi = \pi/3$, the behavior of the 2D atom localization is pretty much similar to that presented in Figs. 3(a) and 3(b). For $\phi = \pi/2$, two craterlike patterns are formed within the half-crater patterns in the first and third quadrants [Fig. 4(c)]. For these cases, the absorption measurement provide little information of the atomic position in the x - y plane. Adjusting $\phi = \pi$, the radii of the craters and half craters are reduced and merge together in the absorption profile so that two craterlike patterns appear in the first and third quadrants, and the atom is localized at the circular edges of the two craters [Fig. 4(d)]. In this case, the uncertainty of the position probability distribution is significantly reduced and the detecting probability of the atom is increased compared to the cases illustrated in Figs. 4(a)–4(c). Yet the spatial resolution of the atom position is still not good enough, so this atom-light coupling condition is not suitable for detecting with high probability in the 2D atom localization.

In the following, we shall analyze another situation aimed at reducing the number of localization peaks in the x - y plane and achieving a unique detecting probability of the atom in the x - y plane. For this purpose, we study interaction of the atom with standing waves.

3. Third case: Only one control field is position dependent

Let us next consider a case where only one of the control fields $\Lambda_{21} = \Lambda_{21}(x, y)$ is position dependent. This field is a combination of two orthogonal standing-wave fields with the same frequency, other laser fields being the traveling waves [Fig. 1(d)]:

$$\begin{aligned}\Lambda_{21} &= \Lambda_{21}(x, y) = \Omega_{21}[\sin(kx) + \sin(ky)], \\ \Lambda_{43} &= \Omega_{43}, \\ \Lambda_{41} &= \Omega_{41}, \\ \Lambda_{32} &= \Omega_{32}.\end{aligned}\quad (25)$$

where no phase factors are contained in the Rabi frequencies Λ_{43} , Λ_{41} , and Λ_{32} by assuming that these fields propagate perpendicular to the x - y plane positioned at $z = 0$.

Let us first explore an impact of the driving fields Ω_{ij} on the position-dependent probe absorption. For $\Omega_{43} = \Omega_{32} = \Omega_{41} = \Omega_{21} = 10\gamma$, the maxima of the probe absorption are situated mainly in the first quadrant, but with a low precision [Fig. 5(a)], i.e., the absorption peak is blurred. The next plots of χ'' are presented for different values of Ω_{ij} . The plots are for $\Omega_{41} = 20\gamma$ and $\Omega_{43} = \Omega_{32} = \Omega_{21} = 10\gamma$ [Fig. 5(b)], for $\Omega_{32} = 20\gamma$ and $\Omega_{43} = \Omega_{41} = \Omega_{21} = 10\gamma$ [Fig. 5(c)], for $\Omega_{43} = 18\gamma$ and $\Omega_{32} = \Omega_{41} = \Omega_{21} = 10\gamma$ [Fig. 5(d)], as well as for $\Omega_{21} = 14.8\gamma$ and $\Omega_{43} = \Omega_{32} = \Omega_{41} = 10\gamma$ [Fig. 5(e)]. It is clear that by increasing each of Ω_{ij} , different spatial distribution and localization patterns are obtained. As one can see in Fig. 5(b), the probe-absorption maxima are distributed on the diagonal in the second and fourth quadrants, with a latticelike pattern showing a uniform position probability distribution across diagonals corresponding to $kx + ky = 2m\pi$ [or $kx - ky = (2n + 1)\pi$] (m, n are integers). When the intensity of driving field Ω_{32} is increased to $\Omega_{32} = 20\gamma$, the maxima of all absorption peaks are located in the third quadrant with a craterlike pattern, and the atom is localized at the circular edge of the crater [Fig. 5(c)]. Increasing the Rabi frequency Ω_{43} to 18γ results in localization of the atom in the first quadrant with a spikelike pattern, whereas in the third quadrant there is a very weak craterlike pattern. Therefore the localization precision of the first quadrant is much higher than that of the third quadrant [Fig. 5(d)]. Although compared to Figs. 5(a)–5(c), in the current situation there is an improvement of the information of the atomic position in the x - y plane, but there is still not a perfect atom localization. A best result appears in Fig. 5(e) in which one can observe that by increasing the intensity of standing-wave field Ω_{21} to 14.8γ the probability of finding the atom is significantly increased and the atom is localized nearly at a certain position [i.e., $(kx, ky) \approx (\pi/2, \pi/2)$]. Therefore, the detection probability of finding the atom in one period of the standing-wave fields reaches almost 100%.

Finally, we discuss the phase dependence of atom localization in the KR5 quantum system for the third situation

described above. Figure 6 displays the atom localization patterns of the probe absorption as a function of the positions (kx, ky) for different values of the relative phase ϕ . When $\phi = 0$, one spikelike localization peak appears in the first quadrant providing the high-precision atom localization [Fig. 6(a)]. In this case, the probability of finding the atom within one period of the standing-wave fields reaches the unity. Adjusting the phase parameter to $\phi = \pi/4$, as it can be seen in Fig. 6(b), the spatial distribution of the probe absorption has a craterlike pattern located in the first quadrant. As we further increase the relative phase to $\phi = \pi/2$, it can be observed from Fig. 6(c) that another craterlike localization peak appears in the third quadrant, so that the peak maxima of the probe absorption exhibits two symmetric craterlike patterns, and the uncertainty of finding an atom in one period increases accordingly. Thus, we can find atom at circular edges around $(kx, ky) \approx (\pi/2, \pi/2)$ or $(kx, ky) \approx (-\pi/2, -\pi/2)$ in quadrants I or III, respectively. For the case $\phi = 3\pi/4$, it can be found from Fig. 6(d) that the localization peak in the first quadrant has completely vanished, and the detection uncertainty is reduced correspondingly. As can be seen in Fig. 6(e), for $\phi = \pi$ the localization peak shifts to the third quadrant and thus, the pattern of the probe absorption becomes a mirror image of the localization pattern for $\phi = 0$ [illustrated in Fig. 6(a)] with respect to the line $y = -x$ in the x - y plane. Therefore, it is quite obvious that the relative phase plays an important role to achieve the perfect detection probability of an atom at a particular position within one period of standing-wave fields.

The origin of such an efficient localization stems from the quantum interference induced by two possible ways of going from the ground level $|5\rangle$ to upper level $|1\rangle$, involving $|5\rangle \xrightarrow{\Omega_p} |3\rangle \xrightarrow{\Omega_{32}} |2\rangle \xrightarrow{\Omega_{21}} |1\rangle$ and $|5\rangle \xrightarrow{\Omega_p} |3\rangle \xrightarrow{\Omega_{43}} |4\rangle \xrightarrow{\Omega_{41}} |1\rangle$ pathways. This affects the absorption of the probe field for such a closed-loop quantum system and results in a perfect atom localization. In Eqs. (10) and (11) for the susceptibility, the quantum interference is represented by the term $2\Lambda_{41}\Lambda_{32}\Lambda_{43}\Lambda_{21}\cos\phi$ playing the main role in formation of the atom localization patterns.

In the first case where the atom-light coupling is described by Eqs. (12) and (13), the interference term reduces $2\Omega_{41}\Omega_{32}\Omega_{43}\Omega_{21}\cos\phi\sin^2(kx)\sin^2(ky)$. The position-dependent absorption spectrum remains then unchanged under the transformations $(x, y) \leftrightarrow (-x, -y)$, $(x, y) \leftrightarrow (x, -y)$, $(-x, y) \leftrightarrow (x, -y)$, and $(-x, y) \leftrightarrow (-x, -y)$. Thus, for a given probe detuning the imaginary part of the susceptibility reads $\chi''(x, y) = \chi''(-x, -y)$, $\chi''(x, y) = \chi''(x, -y)$, $\chi''(-x, y) = \chi''(x, -y)$, and $\chi''(-x, y) = \chi''(-x, -y)$. In such a situation the probe absorption is the same in each of four quadrants, so the localization is not perfect.

In the second case described by Eqs. (14) and (15), the quantum interference term reads $2\Omega_{41}\Omega_{32}\Omega_{43}\Omega_{21}\cos\phi[\sin(kx) + \sin(ky)]^4$. The resulting probe absorption spectrum is invariant only with respect to the transformations $(x, y) \leftrightarrow (-x, -y)$, and $(-x, y) \leftrightarrow (x, -y)$, giving $\chi''(x, y) = \chi''(-x, -y)$, and $\chi''(-x, y) = \chi''(x, -y)$. Consequently the probability distribution is the same in quadrants I and III, as well as in quadrants II and IV, leading to a higher detection probability than in the first case. Finally, in the third case of the atom-light coupling corresponding to Eq. (25), the interference term reads $2\Omega_{41}\Omega_{32}\Omega_{43}\Omega_{21}\cos\phi[\sin(kx) + \sin(ky)]$. In such

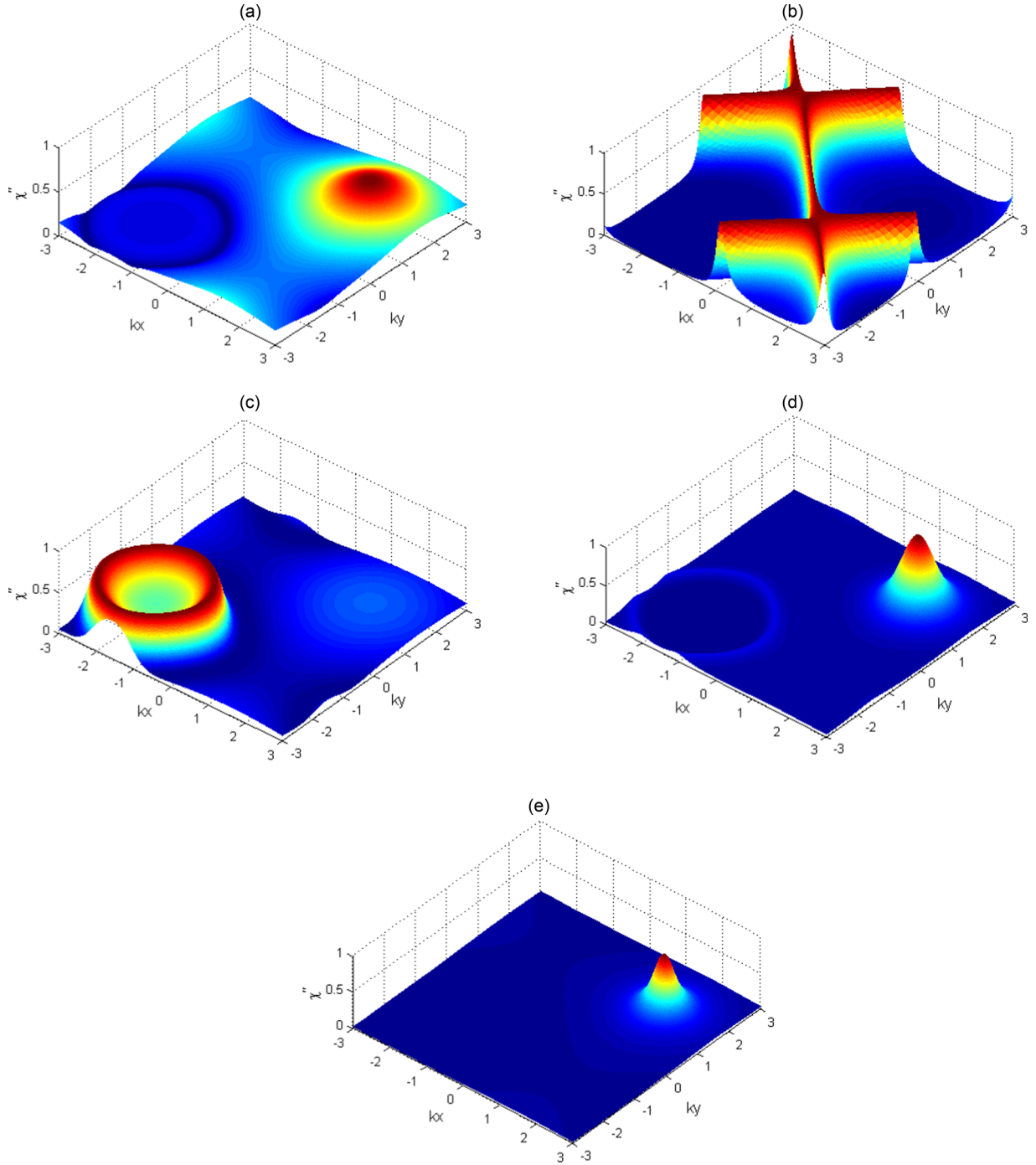


FIG. 5. Plots of probe absorption χ'' versus (kx, ky) . The selected parameters are $(\Omega_{43}, \Omega_{32}, \Omega_{41}, \Omega_{21}) =$ (a) $(10\gamma, 10\gamma, 10\gamma, 10\gamma)$, (b) $(10\gamma, 10\gamma, 20\gamma, 10\gamma)$, (c) $(10\gamma, 20\gamma, 10\gamma, 10\gamma)$, (d) $(18\gamma, 10\gamma, 10\gamma, 10\gamma)$, and (e) $(10\gamma, 10\gamma, 10\gamma, 14.8\gamma)$. Here, $\Delta_{12} = \Delta_{14} = \Delta_{23} = \Delta_{43} = 10\gamma$, $\Delta_p = 0$, and the other parameters are the same as Fig. 4.

a situation there is no symmetry under which the interference term (and hence the position-dependent absorption spectrum) could remain unchanged. The probability distribution of the absorption peaks is then not equal in all four quadrants, so one arrives at a nearly perfect atom localization by properly adjusting the system parameters, as one can see in Figs. 5(d), 6(a), and 6(e).

Let us now discuss the phase effects. When the relative phase of applied fields is $\phi = \pi/2$, the interference term

vanishes in Eqs. (10) and (11). In the third case the probe absorption spectrum then does not alter under the transformation $(x, y) \leftrightarrow (-x, -y)$, giving $\chi''(x, y; \phi = \pi/2) = \chi''(-x, -y; \phi = \pi/2)$. Therefore, one should observe two absorption maxima with the same probability distribution in the quadrants I and III [see Fig. 6(c)]. On the other hand, for $\phi = 0$ and $\phi = \pi$ the interference term becomes maximum. Thus the absorption spectrum remains again unchanged under the transformation $(x, y, \phi = 0) \leftrightarrow (-x, -y, \phi = \pi)$. That is

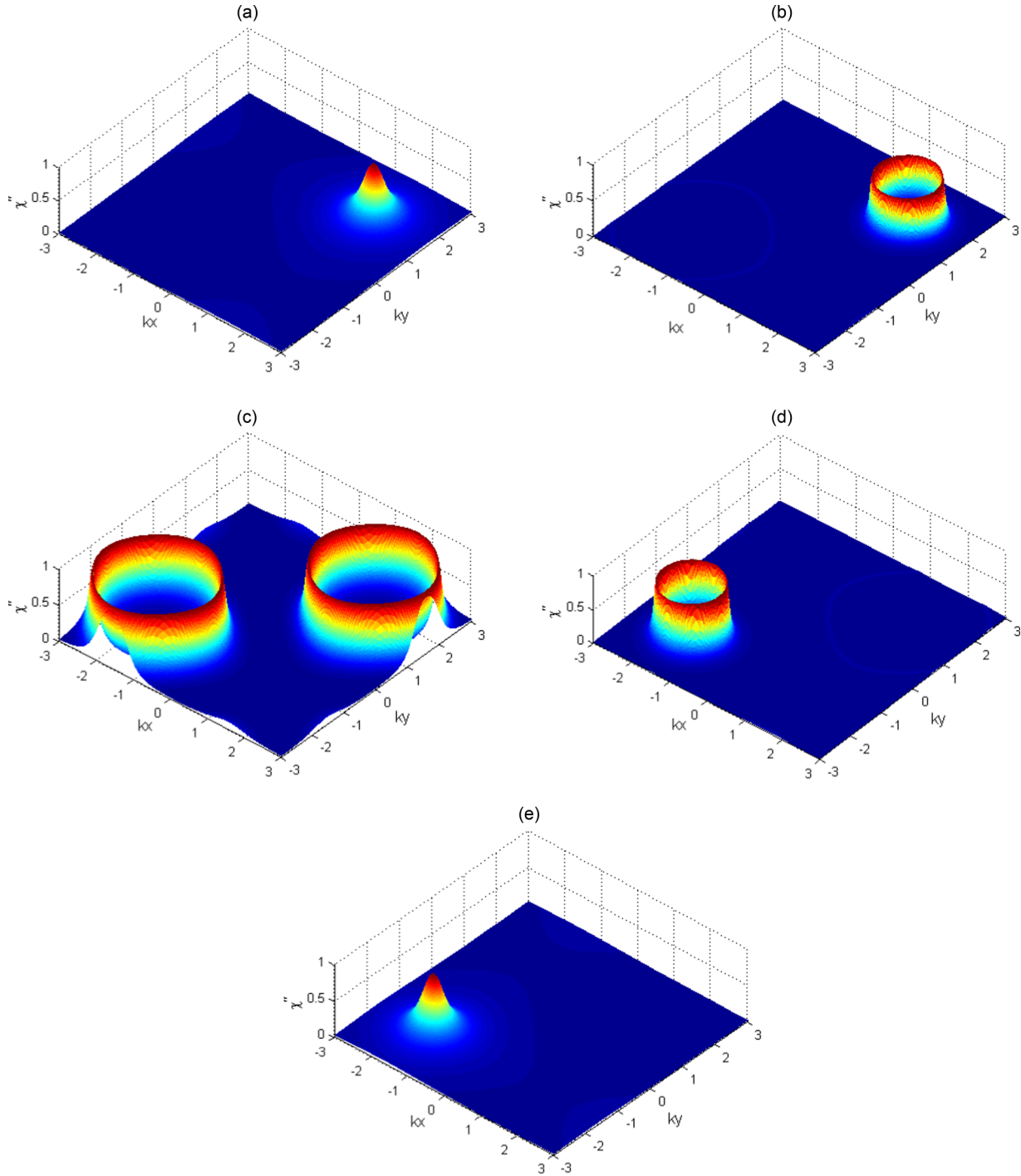


FIG. 6. Plots of probe absorption χ'' versus (kx, ky) . The selected parameters are (a) $\phi = 0$, (b) $\phi = \pi/4$, (c) $\phi = \pi/2$, (d) $\phi = 3\pi/4$, (e) $\phi = \pi$. Here, $(\Omega_{43}, \Omega_{32}, \Omega_{41}, \Omega_{21}) = (10\gamma, 10\gamma, 10\gamma, 14.8\gamma)$. The other selected parameters are the same as Fig. 5.

why for $\phi = \pi$ the probe absorption becomes a mirror image of the localization pattern for $\phi = 0$, as one can see in Figs. 6(a) and 6(e).

B. 3D atom localization

Let us now investigate the phase control of atom localization in three dimensions for our proposed scheme. For this situation, each standing-wave field is obtained from a superposition of three orthogonal standing-wave fields with the same

frequency [Fig. 1(e)]. The Rabi-frequencies corresponding to such standing waves read

$$\begin{aligned}\Lambda_{43} &= \Lambda_{43}(x, y, z) = \Omega_{43} f_3(x, y, z), \\ \Lambda_{41} &= \Lambda_{41}(x, y, z) = \Omega_{41} f_3(x, y, z), \\ \Lambda_{32} &= \Lambda_{32}(x, y, z) = \Omega_{32} f_3(x, y, z), \\ \Lambda_{21} &= \Lambda_{21}(x, y, z) = \Omega_{21} f_3(x, y, z),\end{aligned}\tag{26}$$

with

$$f_3(x, y, z) = \sin(kx) + \sin(ky) + \sin(kz).\tag{27}$$

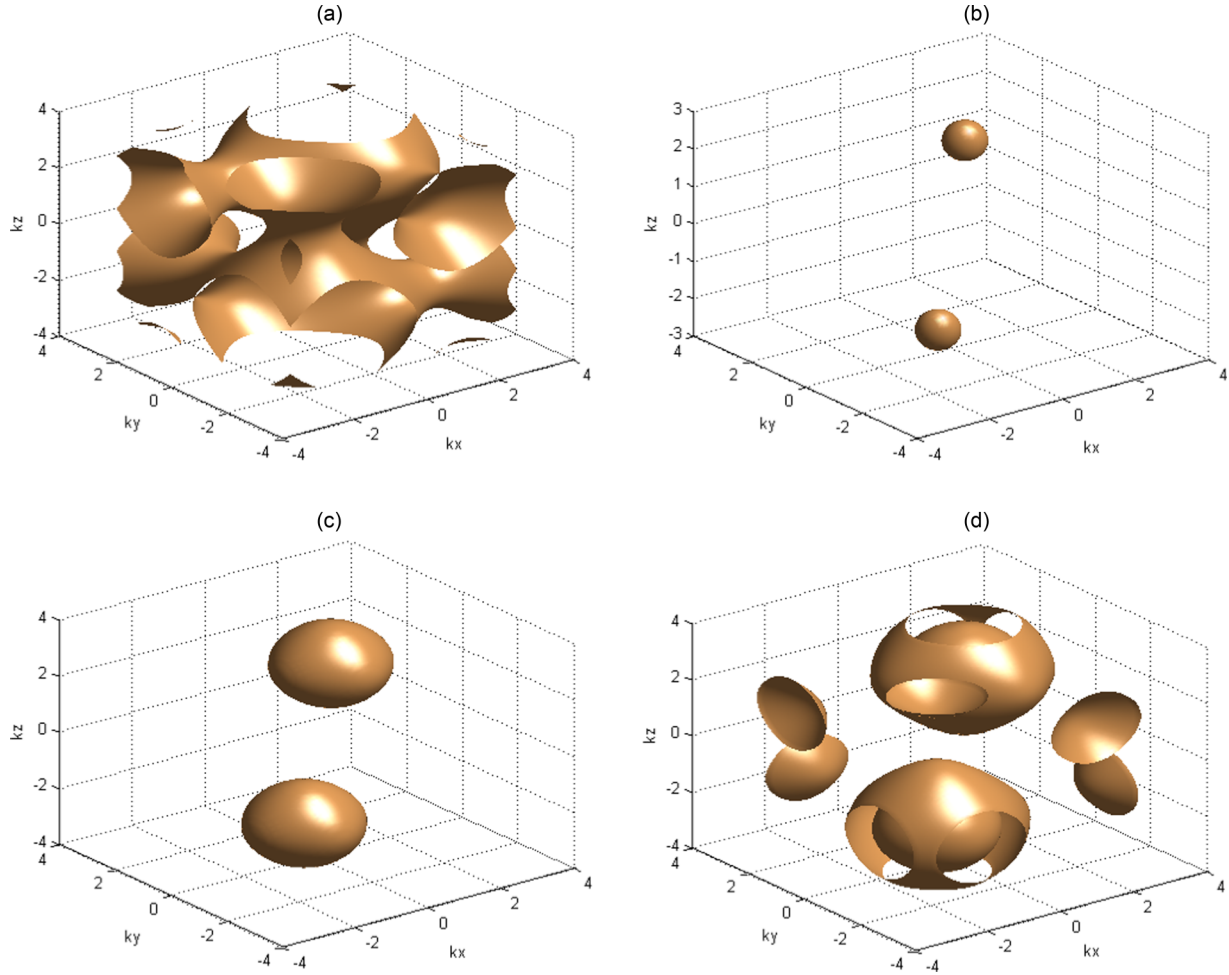


FIG. 7. Isosurface plots of probe absorption χ'' versus (kx, ky, kz) . The selected parameters are (a) $\phi = 0$, (b) $\phi = \pi/3$, (c) $\phi = \pi/2$, and (d) $\phi = \pi$. Here, $(\Omega_{43}, \Omega_{32}, \Omega_{41}, \Omega_{21}) = (10\gamma, 10\gamma, 10\gamma, 10\gamma)$, $\Delta_{12} = \Delta_{14} = \Delta_{23} = \Delta_{43} = \Delta_p = 10\gamma$. The other selected parameters are the same as Fig. 3.

One can see from Eqs. (10) and (11) that the atom localization in 3D space depends crucially on the atom-field coupling featured in Eq. (26) via the relative phase factor ϕ . Figure 7 illustrates the isosurface plot of the probe absorption as a function of the position (kx, ky, kz) for different values of the relative phase ϕ . It can be observed that the effect of the relative phase ϕ leads to different absorptions structures in 3D space. When $\phi = 0$, the probe absorption is distributed in eight different subspaces of the 3D space [Fig. 7(a)]. In particular, we observe that for $\phi = \pi/3$, two spheres appear in the subspaces $0 \leq kx, ky, kz \leq \pi$ and $-\pi \leq kx, ky, kz \leq 0$ with maximum detecting probability of the atom in one of these regions being approximately 1/2 [Fig. 7(b)]. By setting the relative phase ϕ to $\pi/2$, the volume of two spheres in each subspace becomes larger as can be seen in Fig. 7(c) so that the uncertainty in position measurement of the atom is increased. Finally for $\phi = \pi$, the probe absorption spectrum is mostly located in the subspaces $0 \leq kx, ky, kz \leq \pi$ and $-\pi \leq kx, ky, kz \leq 0$ with little in the other regions. Therefore, we could show that different 3D localization patterns can be obtained in 3D space through manipulating the relative phase ϕ . However, the maximum detection probability of finding the atom in the particular region is around 1/2 for the atom-field coupling described by Eq. (26). Note that in this 3D

scheme, the probe field Ω_p is assumed to propagate along the z direction allowing us to monitor the 3D localization of an atom [44].

IV. CONCLUDING REMARKS

In conclusion, we have proposed a scheme of high-precision 2D and 3D atom localization in a five-level atom-light coupling configuration. A pair of atomic internal states are coupled to another pair of states via four strong laser components in all possible pathways in a closed-loop (ring coupling) configuration of the atom-light coupling. We are considering situations where one or more radiation field is position dependent, so the imaginary part of the probe susceptibility is also position dependent. Therefore, it is possible to acquire information about the position of atom through measuring the resulting absorption spectra. Specifically, the effect of the relative phase of the applied fields due to the closed-loop structure of the diamond-shaped subsystem has been explored. An analytical solution is presented to elucidate such a phase sensitivity. It is found that there exists a significant phase dependence of the eigenvalues required to obtain maxima in the probe absorption spectrum. Through appropriate adjusting of the amplitudes and phases of the driving fields, the atom-light Hamiltonian

can experience three, four, and two eigenstates, leading to different localization patterns for the atom. The situations for the optimum atom localization have been identified.

The proposed scheme involving the five-level KR5 structure can be experimentally implemented using the ^{87}Rb atoms. The ground level |5) can be assigned to the state $5S_{1/2}$. The level |3) can be attributed to the $5P_{3/2}$. Two intermediate levels |2) and |4) can be assigned to either the fine structure of the $4D_{3/2}$ substate or the $4D_{5/2}$ substate, as long as the dipole transition

selection rules on the F quantum number is satisfied (the same F quantum number for the intermediate states). The top level |1) can be chosen to the $6P_{3/2}$ state.

ACKNOWLEDGMENTS

The presented work has been supported by the Lithuanian Research Council (No. VP1-3.1-ŠMM-01-V-03-001).

-
- [1] W. Heisenberg, *Zeitschrift für Physik* **43**, 172 (1927).
- [2] A. V. Gorshkov, L. Jiang, M. Greiner, P. Zoller, and M. D. Lukin, *Phys. Rev. Lett.* **100**, 093005 (2008).
- [3] H. Li, V. A. Sautenkov, M. M. Kash, A. V. Sokolov, G. R. Welch, Y. V. Rostovtsev, M. S. Zubairy, and M. O. Scully, *Phys. Rev. A* **78**, 013803 (2008).
- [4] J. A. Miles, Z. J. Simmons, and D. D. Yavuz, *Phys. Rev. X* **3**, 031014 (2013).
- [5] J. R. Gardner, M. L. Marable, G. R. Welch, and J. E. Thomas, *Phys. Rev. Lett.* **70**, 3404 (1993).
- [6] K. T. Kapale, S. Qamar, and M. S. Zubairy, *Phys. Rev. A* **67**, 023805 (2003).
- [7] J. Mompart, V. Ahufinger, and G. Birkl, *Phys. Rev. A* **79**, 053638 (2009).
- [8] S. Qamar, S.-Y. Zhu, and M. S. Zubairy, *Phys. Rev. A* **61**, 063806 (2000).
- [9] E. Paspalakis and P. L. Knight, *Phys. Rev. A* **63**, 065802 (2001).
- [10] M. Sahrjai, H. Tajalli, K. T. Kapale, and M. S. Zubairy, *Phys. Rev. A* **72**, 013820 (2005).
- [11] G. S. Agarwal and K. T. Kapale, *J. Phys. B: At. Mol. Opt. Phys.* **39**, 3437 (2006).
- [12] J. Xu, Q. Li, W. Chao Yan, X. Dong Chen, and X. Ming Hu, *Phys. Lett. A* **372**, 6032 (2008).
- [13] E. Arimondo, *Prog. Opt.* **35**, 257 (1996).
- [14] S. E. Harris, *Phys. Today* **50**, 36 (1997).
- [15] M. D. Lukin, *Rev. Mod. Phys.* **75**, 457 (2003).
- [16] Y. Wu and X. Yang, *Phys. Rev. A* **71**, 053806 (2005).
- [17] M. Fleischhauer, A. Imamoglu, and J. P. Marangos, *Rev. Mod. Phys.* **77**, 633 (2005).
- [18] J. Dalibard, F. Gerbier, G. Juzeliūnas, and P. Öhberg, *Rev. Mod. Phys.* **83**, 1523 (2011).
- [19] A. Kuzmich, A. Dogariu, L. J. Wang, P. W. Milonni, and R. Y. Chiao, *Phys. Rev. Lett.* **86**, 3925 (2001).
- [20] A. Schweinsberg, N. N. Lepeshkin, M. Bigelow, R. Boyd, and S. Jarabo, *Europhys. Lett.* **73**, 218 (2005).
- [21] P. W. Milonni, *Fast Light, Slow Light, Left-Handed Light* (Institute of Physics, Bristol, 2005).
- [22] V. Kudriašov, J. Ruseckas, A. Mekys, A. Ekers, N. Bezuglov, and G. Juzeliūnas, *Phys. Rev. A* **90**, 033827 (2014).
- [23] J.-H. Li, X.-Y. Lü, J.-M. Luo, and Q.-J. Huang, *Phys. Rev. A* **74**, 035801 (2006).
- [24] Z. Wang, A.-X. Chen, Y. Bai, W.-X. Yang, and R.-K. Lee, *J. Opt. Soc. Am. B* **29**, 2891 (2012).
- [25] H. Wang, D. Goorskey, and M. Xiao, *Phys. Rev. Lett.* **87**, 073601 (2001).
- [26] H. R. Hamed and G. Juzeliūnas, *Phys. Rev. A* **91**, 053823 (2015).
- [27] Ying and X. Yang, *Phys. Rev. A* **70**, 053818 (2004).
- [28] Y. Zhang, A. W. Brown, and M. Xiao, *Phys. Rev. A* **74**, 053813 (2006).
- [29] W.-X. Yang, A.-X. Chen, L.-G. Si, K. Jiang, X. Yang, and R.-K. Lee, *Phys. Rev. A* **81**, 023814 (2010).
- [30] V. Ivanov and Y. Rozhdestvensky, *Phys. Rev. A* **81**, 033809 (2010).
- [31] C. Ding, J. Li, X. Yang, D. Zhang, and H. Xiong, *Phys. Rev. A* **84**, 043840 (2011).
- [32] C. Ding, J. Li, Z. Zhan, and X. Yang, *Phys. Rev. A* **83**, 063834 (2011).
- [33] R.-G. Wan, J. Kou, L. Jiang, Y. Jiang, and J.-Y. Gao, *J. Opt. Soc. Am. B* **28**, 622 (2011).
- [34] R.-G. Wan, J. Kou, L. Jiang, Y. Jiang, and J.-Y. Gao, *J. Opt. Soc. Am. B* **28**, 10 (2011).
- [35] Z. Wang, B. Yu, J. Zhu, Z. Cao, S. Zhen, X. Wu, and F. Xu, *Ann. Phys. (NY)* **327**, 1132 (2012).
- [36] J. Lia, R. Yub, M. Liu, C. Ding, and X. Yang, *Phys. Lett. A* **375**, 3978 (2011).
- [37] Rahmatullah and S. Qamar, *Phys. Rev. A* **88**, 013846 (2013).
- [38] R.-G. Wan, T.-Y. Zhang, and J. Kou, *Phys. Rev. A* **87**, 043816 (2013).
- [39] T. Shui, Z. Wang, and B. Yu, *Quantum. Inf. Process* **14**, 929 (2014).
- [40] Z. Wang and B. Yu, *Laser Phys. Lett.* **11**, 035201 (2014).
- [41] J. C. Wu and B. Q. Ai, *Europhys. Lett.* **107**, 14002 (2014).
- [42] D. Zhang, R. Yu, J. Li, X. Hao, and X. Yang, *Opt. Commun.* **321**, 138 (2014).
- [43] Y. Qi, F. Zhou, T. Huang, Y. Niu, and S. Gong, *J. Mod. Opt.* **59**, 1092 (2012).
- [44] V. S. Ivanov, Y. V. Rozhdestvensky, and K.-A. Suominen, *Phys. Rev. A* **90**, 063802 (2014).
- [45] Z. Wang and B. Yu, *J. Opt. Soc. Am. B* **32**, 1281 (2015).
- [46] M. N. Kobrak and S. A. Rice, *Phys. Rev. A* **57**, 2885 (1998).
- [47] K. Bergmann, K. H. Theuer, and B. W. Shore, *Rev. Mod. Phys.* **70**, 1003 (1998).
- [48] F. Vewinger, B. W. Shore, and K. Bergmann, *Adv. At. Mol. Opt. Phys.* **58**, 113 (2010).
- [49] J. Gong and S. A. Rice, *J. Chem. Phys.* **120**, 9984 (2004).
- [50] M. Sugawara, *Chem. Phys. Lett.* **428**, 457 (2006).
- [51] M. S. I. Pierre Meystre, *Elements of Quantum Optics* (Springer, Berlin, 1999).
- [52] M. O. Scully and M. S. Zubairy, *Quantum Optics* (Cambridge University Press, Cambridge, UK, 1997).
- [53] D. L. Campbell, G. Juzeliūnas, and I. B. Spielman, *Phys. Rev. A* **84**, 025602 (2011).